Irreducible Motion Planning by Exploiting Linear Linkage Structures

Andreas Orthey, Olivier Roussel, Olivier Stasse, Michel Taïx

Irreducible Motion Planning by Exploiting Linear Linkage Structures

Andreas Orthey[1], Olivier Roussel[1], Olivier Stasse[1], Michel Taïx[1]

***Abstract*—Irreducibility is a theoretical framework for completeness-preserving dimensionality reduction in motion planning. While classical motion planning searches the full space of continuous trajectories, irreducible motion planning searches the space of minimal swept volume trajectories, called the irreducible trajectory space. We prove that planning in the irreducible trajectory space preserves completeness. We then apply this theoretical result to linear linkage structures, which can be found in several mechanical systems, among them humanoid robots. Our main result establishes that we can reduce the dimensionality of linear linkages in the case where the first link moves on curvature-constrained curves. We further develop a curvature projection method, which can be shown to be curvature-complete, a weaker version of general completeness. As an application, we consider the simplification of humanoid motion planning by considering the arms and legs as linear linkages.**

***Index Terms*—Motion Planning, Irreducible Trajectories, Linear Linkages, Swept Volume, Humanoid Robotics**

I. Introduction

Motion planning is concerned with finding arbitrary motions for arbitrary mechanical systems in arbitrary environments. One important special case is the problem of finding a feasible motion for a humanoid robot in arbitrary environments. An understanding of this case would allow humanoid robots to autonomously accomplish a variety of tasks ranging from elderly care over nuclear waste removal to space exploration.

In this paper, we will investigate a specific property of mechanical systems which we call irreducibility. Irreducibility classifies configuration space trajectories into two categories: reducible and irreducible trajectories. An irreducible trajectory is a trajectory with a minimal swept volume in the environment. We will proof here the important fact that planning with only irreducible trajectories preserves completeness. It follows that motion planning can be conducted entirely inside the irreducible trajectory space.

However, it is not obvious how one would analytically define this irreducible trajectory space. Here, we therefore concentrate on a specific mechanical structure, the linear linkage, and investigate how irreducibility can be defined on it. We note that linear linkages are prevalent in a variety of mechanical systems, which are all consequently susceptible to our reduction concept. Four examples are shown in Fig. 1, a

This research has received funding from the European Union Seventh Framework Programme (FP7/2007 - 2013) under grant agreement n° 611909, KoroiBot.

[1] are with the CNRS, LAAS,7 av. du Colonel Roche, F-31400, Toulouse, France, Univ de Toulouse, LAAS, F-31400, Toulouse, France
{aorthey,oroussel,ostasse,mtaix} at laas.fr

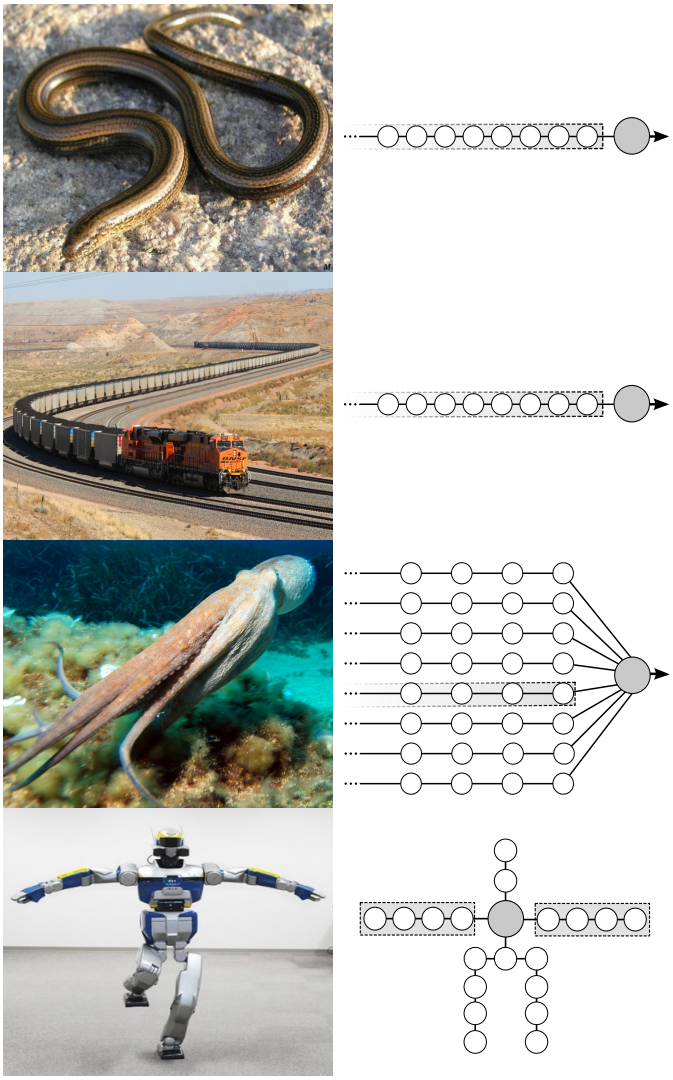

Fig. 1: Examples of free linear linkages in mechanical systems. On the left are different mechanical systems, and on the right is the abstracted idealized linkage structure. **Top**: a snake has one linear linkage with the head as a root link. **Top Middle**: a train has one linkage with the locomotive as the root link. **Bottom Middle**: an octopus has eight arms, each is one linear linkage with the head as a common root link. **Bottom**: humanoid robot HRP-2 has two linear linkages for its arms (with the chest as root link), and two linear linkages for its legs (with the hip as root link).
@Photograph Courtesy:

- Marek Bydg. *Anguis Fragilis Slowworm*. 2004. Poland. http://en.wikipedia.org/wiki/Anguis_fragilis. Web. Accessed April 28th, 2015.
- Unknown Author. *BNSF ES44Ac leading a coal train through S-curve in Powder River Basin*. 2013. Colorado, US. http://www.4rail.net. Web. Accessed April 28th, 2015.
- Albert Kok. Octopus Vulgaris. 2007. Location Unknown. http://en.wikipedia.org/wiki/Octopus. Web. Accessed April 28th, 2015.
- Vincent Fournier. HRP-2 #1 [Kawada], Promet Developed by AIST, 2010. Tochigi, Japan. http://www.vincentfournier.co.uk. Web. Accessed April 28th, 2015.

snake and a train with each one linear linkage, an octopus with eight linear linkages and a humanoid robot with four linear linkages.

This work is based on previous published results in [1]. In particular, Sec. III and parts of the experimental results have been already published. Our additional contributions are

- Introduced the irreducibility property for linear linkages
- Introduced the concept of curvature completeness
- Proved that linear linkages are curvature complete for a specific functional space
- Developed a linear-time irreducibility projection algorithm for linear linkages in 3d.
- Conducted simulated experiments for the humanoid robot HRP-2

In terms of prerequisites, we will assume a rudimentary knowledge of differential geometry in our proofs, as can be found for example in [2].

After summarizing related work in Sec. II, we provide definitions and proofs of the main theorems of irreducible motion planning in Sec. III. Our main result is summarized in Corollary 2, which provides a proof of completeness for irreducible trajectories.

After those preliminaries, we concentrate on linear linkage structures in Sec. IV. We provide a definition of linear linkages and we proof conditions under which we can ignore certain parts of the linkage. This brings us to the concept of a curvature complete algorithm, for which we design in Sec. V a linear-time algorithm in the number of links. In Sec. VI, we finally conduct a set of experiments for a swimming snake robot in simulation and for the real humanoid robot platform HRP-2.

II. Related Work

Motion planning for humanoid robots is a well studied field [3], which has demonstrated its potential in the DARPA Robotics Challenge (DRC) in 2015. Humanoid robots are able to solve difficult tasks, like manipulation planning in kitchen environments [4], contact planning in constrained environments [5], or ladder climbing tasks [6]. Techniques for solving those problems range from optimal control planning [7] over motion database approaches [8] to fast contact planning by identifying convex surfaces [9].

The mechanism and locomotion system for snake robots has long been studied [10]. However, path planning for snake robots has been investigated in relatively few papers. Some of them are classical approaches using numerical potential field [11], genetic algorithms [12] or Generalized Voronoi Graph [13]. The idea of a simplified model is studied by [14], who define a frame that is consistent with the overall shape of the robot in all configurations. In [15] the authors plan a trajectory only for a portion of the snake robot.

Ultimately, all those approaches try to exploit structure to reduce the computational complexity of the problem. In this paper, we concentrate on dimensionality reduction techniques, which have been extensively studied in the motion planning literature. Dalibard et al. [16] have used a principal component analysis (PCA) to bias random sampling. In the context of manipulation motion planning, the powerful eigengrasps [17] [18] have been introduced to identify a low-dimensional representation of grasping movements. Reduction techniques have been especially used in cable motion planning. Mahoney et al. [19] perform a PCA for a high-dimensional cable robot by sampling deformations. Kabul et al. [20] plan the motion of a cable by first planning a motion for the head. Those works showed remarkable results, and demonstrate the effectiveness of reduction techniques. Our work is complementary, in that we are undertaking a formal treatment of conditions under which dimensionality reduction can be performed.

In particular, we show in our work a connection between the curvature and the dimensionality of the problem. Curvature constrained curves have been investigated in the framework of computational geometry [2]. For example, Bereg et al. [21] introduce the term reducibility in the context of sweeping of disks along a planar curve. Our work generalizes this concept by giving completeness guarantees of curves which are non-reducible or as we call it irreducible.

Ahn et al. [22] developed algorithms to compute the reachable regions for curvature constraint motions inside convex polygons. Our work builds upon their theoretical contribution to proof when a system is irreducible.

Guha et al. [23] discuss curvature and torsion constraint on space curves in the context of data point approximation. This work hints at a generalization of our ideas in Sec. IV-F, which we left as a conjecture.

Finally, we use the result described in [24], who showed that a dynamical humanoid robot is small-space controllable, i.e. we can minimize the oscillations of the upper body — and thereby the swept volume — by minimizing its step-size and its step-period. Taking this towards the extreme, the Center-Of-Mass trajectory can be planned as if the robot was sliding on the floor. This sliding motion can be seen as an irreducible motion and thereby provides a first necessary condition for feasibility.

III. Irreducible Trajectories

We restate relevant motion planning definitions, following the classical formulation by [25, Chapter 4]

Definition 1 (Motion Planning Problem)**.** *Let* $A = \{\mathcal{R}, \mathcal{C}, q_I, q_G, \mathbf{E}\}$ *be a motion planning problem, with* $\mathcal{R}$ *the robotic system,* $\mathcal{C}$ *the configuration space,* q_I *the initial configuration,* q_G *the goal configuration, and* $\mathbf{E}$ *the environment.*

Definition 2 (Configuration Space Trajectory)**.** *Let* A *be given. Then we denote by* $\mathcal{F}(q_I, q_G) = C^1([0,1], \mathcal{C})$ *the set of continuously differentiable functions from* $[0,1]$ *to the configuration space* $\mathcal{C}$*, with the property that if* $\tau \in \mathcal{F}(q_I, q_G) \Rightarrow \tau(0) = q_I, \tau(1) = q_G$.

Definition 3 (Swept Volume)**.** *The workspace volume swept by the trajectory* $\tau \in \mathcal{F}(q_I, q_G)$ *will be denoted by* $\mathcal{SV}(\tau)$.

Definition 4 (Feasible Trajectory)**.** *A trajectory* $\tau \in \mathcal{F}(q_I, q_G)$ *is called feasible in an environment* $\mathbf{E}$*, if* $\mathcal{SV}(\tau) \cap \mathbf{E} = \emptyset$.

Definition 5 (Feasible Configuration Space Trajectory)**.** *Let* $\mathbf{S} \subset \mathcal{F}(q_I, q_G)$ *be a set of Configuration space trajectories.*

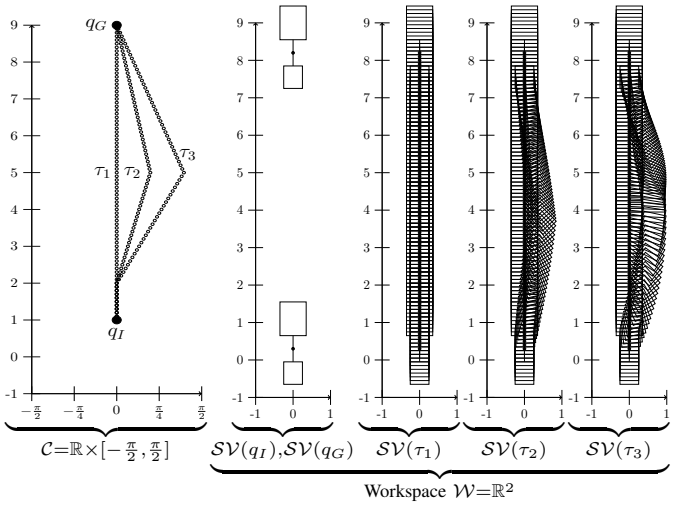

Fig. 2: Explanatory example of irreducible trajectories for a 2-link, 2-dof robot, which can move along the y-axis, and which has one rotational joint between its two links, such that its configuration space is $\mathcal{C} = \mathbb{R} \times [-\frac{\pi}{2}, \frac{\pi}{2}]$. **Left.** Three configuration space trajectories τ_1, τ_2, τ_3 with $\tau_1(0) = \tau_2(0) = \tau_3(0) = q_I$, $\tau_1(1) = \tau_2(1) = \tau_3(1) = q_G$. **Right.** The workspace volume of the starting configurations q_I, q_G, and the swept volume of the three trajectories, whereby we have that $\mathcal{SV}(\tau_1) \subset \mathcal{SV}(\tau_2)$ and $\mathcal{SV}(\tau_1) \subset \mathcal{SV}(\tau_3)$, i.e. τ_2 and τ_3 are reducible by τ_1, and τ_1 is in fact irreducible. Adapted from [1].

Let A be a specific motion planning problem. If there exist $\tau \in \mathbf{S}$ such that τ solves A, then $\mathbf{S}$ is said to be feasible w.r.t. A.

We denote by $\subset$ the proper subset. Let $A = \{\mathcal{R}, \mathcal{C}, q_I, q_G, \mathbf{E}\}$ be given, and let $\mathcal{F} = \mathcal{F}(q_I, q_G)$.

Definition 6. *A trajectory $\tau' \in \mathcal{F}$ is called reducible, if there exist $\tau \in \mathcal{F}$ such that $\mathcal{SV}(\tau) \subset \mathcal{SV}(\tau')$. Otherwise τ' is called* irreducible.

Fig. 2 provides a visualization of the irreducible definition for trajectories. We show three configuration space trajectories τ_1, τ_2, τ_3, and its swept volumes in workspace. Applying the definition, we have that τ_2 and τ_3 are reducible by τ_1. We will now show why irreducibility is important for motion planning.

Theorem 1. *Let $\tau, \tau' \in \mathcal{F}$ be such that $\mathcal{SV}(\tau) \subset \mathcal{SV}(\tau')$, i.e. τ' is reduced by τ.*

$$\textit{If } \tau \textit{ is infeasible} \Rightarrow \tau' \textit{ is infeasible}$$
$$\textit{If } \tau' \textit{ is feasible} \Rightarrow \tau \textit{ is feasible}$$

Proof in Appendix.

Definition 7 (Irreducible Trajectories)**.** *Let the set of all irreducible configuration space trajectories be defined as*

$$\mathcal{I} = \{\tau \in \mathcal{F} | \tau \textit{ is irreducible}\} \tag{1}$$

Lemma 1. *Let $\tau \in \mathcal{F} \setminus \mathcal{I}$. Then there exist $\tau' \in \mathcal{I}$, with $\mathcal{SV}(\tau') \subset \mathcal{SV}(\tau)$.*

Proof in Appendix.

Theorem 2. *If $\mathcal{I}$ is infeasible then $\mathcal{F}$ is infeasible*

Proof in Appendix.

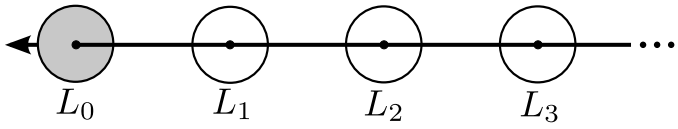

Fig. 3: A free linear linkage with L_0 being the root link, and $L_1, L_2, \cdots$ are called the sublinks. The black arrow gives the movement direction of L_0. In this paper, we will give conditions under which only the root link L_0 has to be planned for, while the sublinks can be ignored while preserving a curvature completeness property.

Corollary 1. *Motion planning is complete in $\mathcal{I}$*

Proof in Appendix.

Going back to the example in Fig. 2, we can now make the statement, that trajectories τ_2 and τ_3 can be ignored for motion planning, while still being complete. This means we now have a formed a geometric argument, which allows us to reduce the dimensionality of a motion planning problem while preserving completeness.

IV. Irreducibility for Linear Linkages

We will now use the theoretical concept of an irreducible trajectory to study linear linkages. A linear linkage is a mechanical system consisting of $N + 1$ links, which are connected in a chain, as depicted in Fig. 3. We will call the first link in the chain the *root link*, denoted by L_0, and the other N links as *sublinks*. If the root link is moveable we call the linear linkage *free*, otherwise non-free. We will exclusively work with free linear linkages with a finite number of sublinks, if not otherwise stated. We will study in this section conditions for movements of L_0, such that we can ignore the sublinks.

This whole section is dedicated to the task of finding conditions on the movement of the root link L_0, such that all sublinks can be ignored for motion planning. Our main idea is that if the root link moves on curvature-constrained curves in $\mathbb{R}^2$, we can always reduce the sublinks, and thereby preserving a weak form of completeness. We will give an informal treatment of this idea, then proceed to proof the case of curvature-constraint motion planning in $\mathbb{R}^2$ and finally discuss the $\mathbb{R}^3$ case, which we leave as a conjecture.

A. Swept Volume of a Train

Let us observe that a train is a linear linkage with the locomotive as a root link, and its N railroad cars as sublinks. If the train moves between two stations on given railroad tracks, then we can state the following: the swept volume of the train with N railroad cars is equal to the swept volume of the train with zero railroad cars. The reason is that we constrain the movement of the locomotive to be bounded by a minimal curve radius. Given a minimal curve radius, we are allowed to construct arbitrary railroad tracks for a train, to move from one city to the next. More abstractly, we can translate this to: we are allowed to construct space curves f from a functional space $\mathcal{F}$, under the constraint that every function f has a bounded curvature.

To come back from our train example to arbitrary mechanical systems, let us call the locomotive a root link, and each railroad car a sublink. Intuitively, if the root link is big enough,

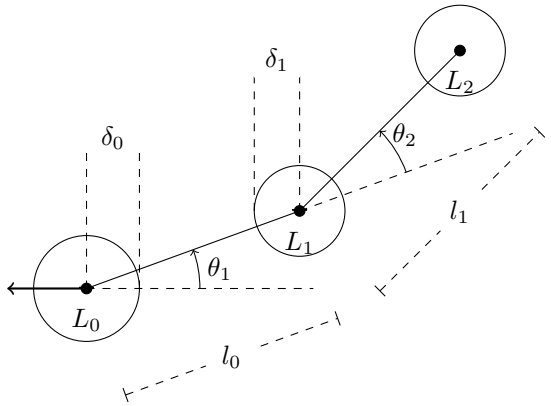

Fig. 4: $N = 2$ linear linkage system

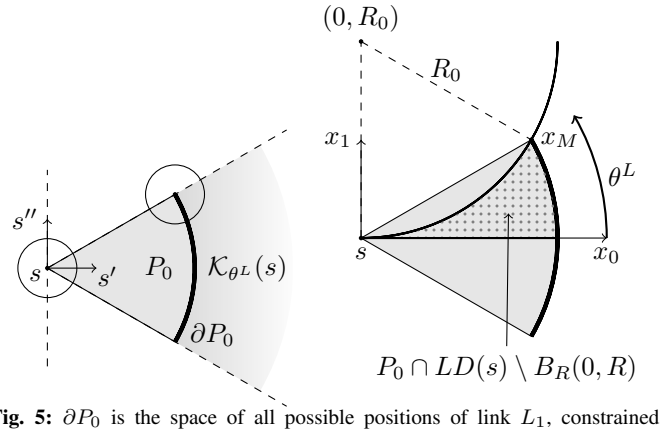

Fig. 5: ∂P_0 is the space of all possible positions of link L_1, constrained by link L_0. We establish in this section that for a specifically constructed functional space $\mathcal{F}_{\kappa_0}$ any function which starts at s and has first derivative equal to s' will leave the area P by crossing ∂P_0.

i.e. the locomotive is bigger than the railroad cars, and if the root link moves on space curves bounded by a certain curvature, then we can state that there exists a configuration of the sublinks, such that the swept volume of the sublinks is a subset of the swept volume of the root link. The big implication here is: if we find a physically feasible railroad track for a locomotive, then we can add a finite number of railroad cars, while still being feasible. A train in this sense is redundant, i.e. there are links which can be ignored for motion planning. Our goal now is to formalize those ideas rigorously. We will start by defining a functional space for the root link L_0, then proof that there always exist configurations for the sublinks $L_1, \cdots, L_N$, such that they are inside of the swept volume of L_0.

B. Curvature Functional Space

Let us consider a $N = 1$ linear linkage with links L_0, L_1 in the plane $\mathbb{R}^2$, connected by a rotational joint at the center of L_0, with distance l_0 to L_1. A $N = 2$ linear linkage is visualized in Fig. 4. The rotational joint has an allowed rotation of $\theta \in [-\theta^L, \theta^L]$. Let us denote by $s = (s_0, s_1) \in \mathbb{R}^2$ the position of L_0, and by s' its orientation. Let us define a cone $\mathcal{K}_{\theta^L}(s) = \{(x_0, x_1) \in \mathbb{R}^2 | \|x_1 - s_1\|^2 \leq (x_0 - s_0) \tan \theta^L\}$ with apex s, orientation s', and aperture θ^L. Then given L_0 at (s, s'), we can define the set ∂P_0 of all possible positions of L_1 as a circle intersecting $\mathcal{K}_{\theta^L}(s)$ and the corresponding disk segment P_0 as a disk intersecting $\mathcal{K}_{\theta^L}(s)$.

$$\begin{aligned} P_0 &= \{x \in \mathbb{R}^2 | \|x - s\| \leq l_0\} \cap \mathcal{K}_{\theta^L}(s) \\ \partial P_0 &= \{x \in \mathbb{R}^2 | \|x - s\| = l_0\} \cap \mathcal{K}_{\theta^L}(s) \end{aligned} \tag{2}$$

whereby P_0 and ∂P_0 are visualized in Fig. 5.

We will now construct a functional space $\mathcal{F}_{\kappa_0}$ by hand, and then prove that all functions from $\mathcal{F}_{\kappa_0}$ starting at (s, s') will *necessarily* have to leave P_0 by crossing ∂P_0.

Let us define the functional space

$$\mathcal{F}_{\kappa_0} = C^2([0, 1], \mathbb{R}^2) \tag{3}$$

with given $\tau(0) = s$, $\tau'(0) = s'$, $\tau(1) \notin P_0$ and for all $\tau \in \mathcal{F}_{\kappa_0}$ we define a maximum curvature by

$$\kappa_0 = \frac{2 \sin(\theta^L)}{l_0} \tag{4}$$

The curvature κ_0 has been constructed in the following way: first, let us observe that for any point $\tau(t)$ on τ the curvature is defined by $\kappa_0 = \frac{1}{R_0}$ whereby R_0 is the radius of the osculating circle at $\tau(t)$ [2]. We will now consider trajectories parametrized by arc-length, such that $\tau'(t) \cdot \tau''(t) = 0$. The center of the osculating circle has to lie therefore in the direction of vector $\tau''(t)$. We are searching for the minimal ball, which ensures that all functions will necessarily leave P_0 through ∂P_0. This ball touches the most extreme point of ∂P_0, which we call x_M:

$$x_M = (l_0 \cos(\theta^L), l_0 \sin(\theta^L))^T \tag{5}$$

See also Fig. 5 for clarification. The ball can be found by solving the equation

$$\|x_M - (0, R_0)^T\|^2 = R_0^2 \tag{6}$$

The solution is given by

$$R_0 = \frac{l_0}{2 \sin(\theta^L)} \tag{7}$$

Please note that $l_0 \leq 2R_0$, which will be important in the upcoming proof.

C. Reducibility theorems of $\mathcal{F}_{\kappa_0}$

We are now going to proof some elementary properties of this functional space $\mathcal{F}_{\kappa_0}$, which will ultimately show that under certain conditions, we can ignore the sublinks for motion planning. The reader is encouraged to visualize the theorems by thinking about the train example and the maximum curvature under which the swept volume of the cars will be inside the swept volume of the locomotive. Our first theorem builds upon the pocket lemma introduced by [26]. It also uses a slightly modified version of a result by [22, Lemma 6]

Theorem 3. *For all $\tau \in \mathcal{F}_{\kappa_0}$ there exists $t_0 \in [0, 1]$ such that $\tau(t_0) \in \partial P_0$ and $\tau(t) \in P_0$ for all $t \leq t_0$.*

Explanation: every trajectory from our constructed functional space $\mathcal{F}_{\kappa_0}$ will leave the region P_0 by crossing ∂P_0. Visualized in Fig. 6.

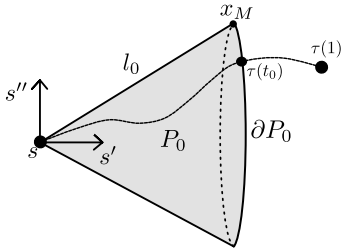

Fig. 6: Cone spanned by the length l_0, the limit angle θ^L and the position of s. Every function from $\mathcal{F}_{\kappa_0}$ will necessarily leave P_0 by crossing ∂P_0 at $\tau(t_0)$ to reach a point $\tau(1)$ outside P_0.

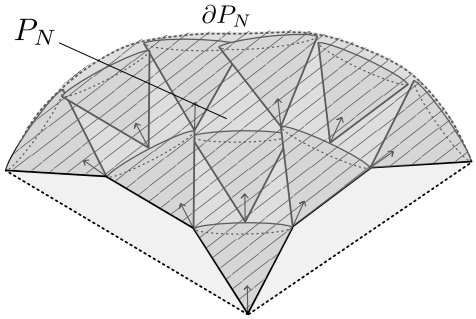

Fig. 7: A succession of cones, spanning the space between s and ∂C_s, which necessarily has to be traversed by any function from $\mathcal{F}_{\kappa_N}$.

Proof: Let us decompose the problem into two parts. First, we consider the left side of s, which we define as $LD(s) = \{(x_0, x_1) \in \mathbb{R}^2 | x_0 \geq 0, x_1 \geq 0\}$. Our proof will first establish that all circles with center $(0, R)$ and radius $R \geq R_0$ will intersect ∂P_0. Second, we use a lemma from [22] to establish that all trajectories from $\mathcal{F}_{\kappa_0}$ will necessarily leave P_0 by crossing ∂P_0, and that there is no trajectory crossing the ball $B_R(0, R)$ for given curvature $\kappa = \frac{1}{R}$.

- We will proof that every circle with center $(0, R)$ and radius $R \geq R_0$ will intersect ∂P_0. By construction we have that the circle R_0 intersects ∂P_0 at the point specified by angle θ^L. We define the angle depending on R by $\theta(R) = \operatorname{asin}\left(\frac{l_0}{2R}\right)$. We want to establish that indeed $\theta^L \geq \theta(R) \geq 0$, i.e. a ball with radius $R \geq R_0$ will always intersect ∂P_0 at a point below x_M and above 0. Since asin is monotone increasing on $[0, 1]$, $l_0, R \geq 0$ and $l_0 \leq 2R$, we have that $\theta(R) \geq 0$. To establish $\theta^L \geq \theta(R)$ we note that given $\operatorname{asin}\left(\frac{l_0}{2R_0}\right) \geq \operatorname{asin}\left(\frac{l_0}{2R}\right)$ we can write $\frac{l_0}{2R_0} \geq \frac{l_0}{2R}$, since asin is monotone increasing. It follows that $R \geq R_0$ as required.
- Let us now construct a polygonal chain for one $R \geq R_0$ in the following way: we start on the boundary of P_0 at point s and follow direction s' until we reach ∂P_0. At ∂P_0 we move upwards on ∂P_0 until we meet the ball with radius R, which intersects ∂P_0. This construct is a polygonal chain and specifically called a forward chain by [22]. This chain follows the boundary of $P_0 \cap LD(s)$. Ergo, we can apply Lemma 6 of [22], which states that if such a forward chain intersects the circle of unit radius, then the reachable region of all trajectories in $\mathcal{F}_{\kappa_0}$ is given by $P_0 \cap LD(s) \setminus B_R(0, R)$ (the unit radius can be obtained by scaling the space). See Fig. 5 for visualization. One interpretation of the pocket lemma from [26] let us now state the following: no trajectory can escape the region $P_0 \cap LD(s) \setminus B_R(0, R)$ except through ∂P_0 or the lower boundary. Since the same arguments apply for the lower part, i.e. with $RD(s) = \{x \in \mathbb{R}^2 | x_0 \geq 0, x_1 \leq 0\}$ instead of $LD(s)$, we can reason that any function from $\mathcal{F}_{\kappa_0}$ starting in s can only escape the region $P_0 \setminus (B_R(0, R) \cup B_R(0, -R)) \subset P_0$ through the arc segment ∂P_0. Since $\tau(1) \notin P_0$, the result follows.

■

This assures that for a moving particle, it will always cross the arc segment ∂P_0. Now we consider the sweeping of disks $D_\delta = \{x \in \mathbb{R}^2 | \|x\| \leq \delta\}$ with radius δ along a trajectory $\tau \in \mathcal{F}_{\kappa_0}$. Let us define $L_0 = D_{\delta_0}(s_0)$, $L_1 = D_{\delta_1}(s_1)$, and $s_1 = (l_0 \cos(\theta), l_0 \sin(\theta))$.

Theorem 4. *Let $L_0 = D_{\delta_0}(s)$. Then there exists $\theta \in [-\theta^L, \theta^L]$ such that for all $\tau \in \mathcal{F}_{\kappa_0}$ there exists $t_0 \in [0, 1]$ such that $L_1 \subset (\tau(t_0) \oplus L_0)$ if $\delta_1 \leq \delta_0$.*

Proof:

Due to Theorem 3 we have that a point starting from s_0 following a trajectory from $\tau \in \mathcal{F}_{\kappa_0}$ will necessarily cross ∂P_0. Let $\tau(t) \in \partial P_0$ be the crossing point. Let us choose $s_1 = \tau(t)$ as the position of link L_1. θ can be recovered by $\theta = \operatorname{acos}\left(\frac{(s_1 - s_0)^T s'}{\|s'\| l_0}\right)$. Now at s_1 we have that the volume of $(\tau(s_1) \oplus L_0)$ is smaller than $(\tau(s_1) \oplus L_1)$ exactly when $\delta_1 \leq \delta_0$.

■

D. Generalization to N sublinks

Let us define a linear linkage in *canonical form* in the following way: Let $L_0, \cdots, L_N \in D^2$ be disk links of radius $\delta_0, \cdots, \delta_N$ connected by lines of equal length $l_0, \cdots, l_{N-1}$ with $l_0 = \cdots = l_{N-1}$, $\delta_i > 0$, $l_i > \delta_i + \delta_{i+1}$, $\delta_i \leq \delta_0$ for all $i \in [0, N]$ and joints limits $\{\{-\theta_0^L, \theta_0^L\}, \cdots, \{-\theta_{N-1}^L, \theta_{N-1}^L\}\}$ with $\theta_0^L = \cdots = \theta_{N-1}^L$. We will refer to this canonical linear linkage structure as $\mathcal{R}_L^N$.

Let us define by P_N the interior of the space spanned by all possible sublink configurations, as depicted in Fig. 7. Let us define analog a functional space $\mathcal{F}_{\kappa_N}$ as

$$\mathcal{F}_{\kappa_N} = C^1([0, 1], \mathbb{R}^2) \tag{8}$$

with $\tau(0) = s$, $\tau'(0) = s'$, $\tau(1) \notin P_N$, and for all $\tau \in \mathcal{F}_{\kappa_N}$ we have a maximum curvature given by

$$\kappa_N = \frac{2 \sin(\theta^L)}{N l_0}, N > 1 \tag{9}$$

E. Irreducibility of Linear Linkage

For $N = 1$, we proved that there exist θ_1 such that $L_1 \in \tau$. For $N > 1$, the tangent t of τ might differ from the normal n of the line $(L_0 L_1)$. We denote the angle between t and n as θ_{D_i}. See Fig. 8 for clarification. To ensure that we can

always find a feasible configuration, such that all links are on τ, we therefore need to ensure that $\theta_i = \theta_{D_i} + \theta_t \leq \theta^L$ for all $i \in [0, N]$.

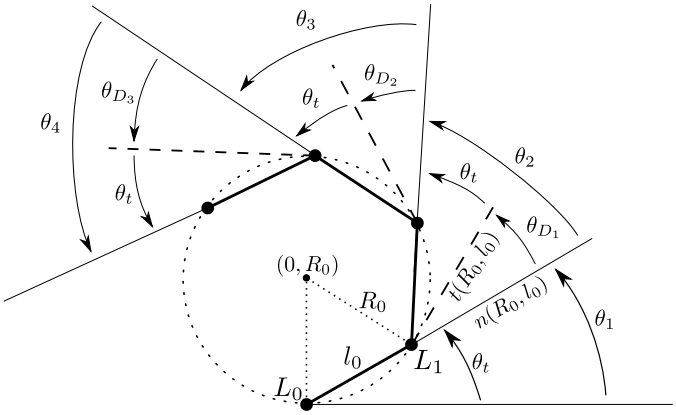

Fig. 8: Linear Linkage along a curve τ. The angle between the tangent to the osculating circle t and the normal n of the line $(L_0 L_1)$ is given by θ_{D_i}. The angle θ_t denotes the maximum angle given a maximal constant curvature κ_N.

For our proofs, we assume two premises to be true.

P1 If $l_0 = l_i$ for all $i \in [1, N]$, then $\theta_{D_1} = \theta_{D_i}$ for all $i \in [1, N]$

P2 Maximum angle between t and n can be found for $\tau = \tau_{\kappa_N}$ with τ_{κ_N} being the constant maximum curvature trajectory with curvature κ_N everywhere.

We now want to determine the angles θ_t,θ_{D_1} depending on the radius R_0 of the osculating circle.

By geometrical arguments of circle-circle intersection [1], we can write

$$\begin{aligned} n(R_0, l_0) &= \begin{pmatrix} \frac{l_0}{2R_0}\sqrt{4R_0^2 - l_0^2} \\ \frac{l_0^2}{2R_0} \end{pmatrix} \\ t(R_0, l_0) &= \begin{pmatrix} \frac{-l_0^2}{2R_0} + R_0 \\ \frac{l_0}{2R_0}\sqrt{4R_0^2 - l_0^2} \end{pmatrix} \end{aligned} \tag{10}$$

$$\begin{aligned} \theta_t &= \arctan\left(\frac{l_0}{\sqrt{4R_0^2 - l_0^2}}\right) \\ \theta_{D_1} &= \arccos\left(\frac{n \cdot t}{\|n\|\|t\|}\right) = \arccos\left(\frac{4R_0^2 - l_0^2}{4R_0^2}\right) \end{aligned} \tag{11}$$

We now choose a certain R_0, and prove that $\theta_t(R_0) + \theta_{D_1}(R_0) \leq \theta^L$. Let

$$R_0 = \frac{N l_0}{2 \sin \theta^L} \tag{12}$$

such that $\mathcal{F}_{\kappa_N}$ is defined by $\kappa_N = \frac{1}{R_0}$.

Lemma 2. *Given premises* **P1**, **P2** *and a trajectory $\tau \in \mathcal{F}_{\kappa_N}$, then for $t \in [0, 1]$ and $\delta_0 = 0, \delta_i = 0$, there exist joint configurations $\theta_1, \cdots, \theta_N$ for the linear linkage $\mathcal{R}_L^N$, such that every L_i is located on τ. Furthermore, the maximum distance between τ and the lines $(L_0 L_1) \cdots (L_{N-1} L_N)$ is given by $d_{\kappa_N} = R_0 - \sqrt{R_0^2 - \frac{l_0^2}{4}}$*

[1]Circle-Circle Intersection – Wolfram Mathworld

Proof: θ_t,θ_{D_1} evaluates to

$$\begin{aligned} \theta_t &= \arctan\left(\frac{\sin \theta^L}{\sqrt{N^2 - \sin^2 \theta^L}}\right) \\ \theta_{D_1} &= \arccos\left(\frac{N^2 - \sin^2 \theta^L}{N^2}\right) \end{aligned} \tag{13}$$

for $N > 1$.

Due to premise **P2**, we know that $\theta_t + \theta_{D_1}(R_0) \geq \theta_t + \theta_{D_1}(R)$ for $R \geq R_0$, and so we can concentrate on the maximum curvature case R_0. Due to premise **P1**, we now only have to prove that $\theta_t + \theta_{D_1} \leq \theta^L$. By induction on N, we get for $N = 2$

$$\begin{aligned} \theta_t(2) &= \arctan\left(\frac{\sin \theta^L}{\sqrt{4 - \sin^2 \theta^L}}\right) \leq \arctan\left(\frac{\sin \theta^L}{2}\right) \\ &\leq \frac{\sin \theta^L}{2} \leq \frac{\theta^L}{2} \\ \theta_{D_1}(2) &= \arccos\left(1 - \frac{\sin^2 \theta^L}{4}\right) = 2 \arctan\left(\frac{2 \sin \theta^L}{8 - \sin^2 \theta^L}\right) \\ &\leq \frac{4 \sin \theta^L}{8 - \sin^2 \theta^L} \leq \frac{4 \sin \theta^L}{8} = \frac{\sin \theta^L}{2} \leq \frac{\theta^L}{2} \end{aligned} \tag{14}$$

whereby we relied on the fact that for $x > 0$ we have $\arctan(x) \leq x$ since $\arctan'(x) = \frac{1}{1+x^2} \leq 1$, for $x > 0$ we have $\sin(x) \leq x$ since $\sin'(x) = \cos(x) \leq 1$, and that $\arccos(x) = 2 \arctan\left(\frac{\sqrt{1-x^2}}{1+x}\right)$.

We now observe that

$$\begin{aligned} \theta_t(N) &= \arctan\left(\frac{\sin \theta^L}{\sqrt{N^2 - \sin^2 \theta^L}}\right) \geq \arctan\left(\frac{\sin \theta^L}{N}\right) \\ &\geq \arctan\left(\frac{\sin \theta^L}{\sqrt{(N+1)^2 - \sin^2 \theta^L}}\right) = \theta_t(N+1) \\ \theta_{D_1}(N) &= \arccos\left(\frac{N^2 - \sin^2 \theta^L}{N^2}\right) \geq \arccos\left(1 - \frac{\sin^2 \theta^L}{N^2}\right) \\ &\geq \arccos\left(1 - \frac{\sin^2 \theta^L}{(N+1)^2}\right) = \theta_{D_1}(N+1) \end{aligned} \tag{15}$$

which shows that $\theta_t(N) + \theta_{D_1}(N) \geq \theta_t(N+1) + \theta_{D_1}(N+1)$. Therefore we have $\theta^L \geq \theta_t(2) + \theta_{D_1}(2) \geq \cdots \geq \theta_t(N) + \theta_{D_1}(N)$ for $N > 1$ as required.

Now given the constant maximum curvature we have that the points $L_0, (0, R_0)$ and L_1 are creating an isosceles triangle. See Fig. 8 for visualization. The maximum distance of the line $(L_0 L_1)$ and the circle can be obtained by the height of the triangle, such that $d_{\kappa_N} = R_0 - \sqrt{R_0^2 - \frac{l_0^2}{4}}$.

■

Theorem 5. *Let $\tau = \tau_I \circ \tau_{\kappa_N} \circ \tau_E$ with $\tau \in \mathcal{F}_{\kappa_N}$ and τ_I, τ_G be the linear extensions of τ. If the root link L_0 moves along τ, then for $\delta_i \leq \delta_0$ and $\frac{l_0^2}{2R_0} \leq \delta_0$, we have that there exists sublink configurations $\theta_1, \cdots, \theta_N$ such that the volume of the linear linkage $\mathcal{R}_L^N$ is a subset of $\tau \oplus L_0$*

Proof: By Lemma 2, the maximum distance of the linear linkage to τ is given by d_{κ_N}. If $\delta_0 \geq d_{\kappa_N}$, then any point on the linear linkage curve will be inside $\tau \oplus L_0$. By Theorem 2 we can choose $\theta_1, \cdots, \theta_N$, such that the center of every L_i is located on τ. Then there exists an instance t such that $L_i = \tau(t)$. L_i is a subset of $\tau \oplus L_0$ exactly if $\delta_0 \geq \delta_i$. ■

We have showed that if the root link of a linear linkage moves on a κ_N-curvature constrained trajectory, then there exists a sublink configuration at every instance, such that all sublinks are inside of the swept volume of the root link.

F. 3-Dimensional Conjecture

In 3 dimensions, a space curve is defined by its curvature and torsion [2]. We will conjecture that our results apply also to 3 dimensions. Let us define the following functional space

$$\mathcal{F}_{\kappa,T} = C^2([0,1], \mathbb{R}^3) \tag{16}$$

with $\tau \in \mathcal{F}_{\kappa,T} \Rightarrow \tau(0) = s, \tau'(0) = s', \tau''(0) = s''$ and that $\tau(1)$ is outside a cone P_0 spanned by s, and the length of the link l_0, as depicted in Fig. 6. The curvature κ and torsion T of τ is constrained to be

$$\kappa = \frac{2\sin(\theta^L)}{l_0}, \quad T \in \mathbb{R} \tag{17}$$

Conjecture 1. *Theorem 5 holds for $\mathcal{F}_{\kappa,T}$ in 3-dimensions.*

We will use this conjecture in our planning algorithm, to verify it experimentally and let the proof for future work.

Finally, we want to point out that completeness is not maintained for $\mathcal{F}_{\kappa,T}$

Theorem 6. *The motion planning problem A for $\mathcal{R}_L^N$ is not complete in $\mathcal{F}_{\kappa,T}$*

Proof: Since we constraint the functional space to not allow functions with curvatures $> \kappa$, we can trivially construct a counterexample in the following way: let us consider a disk $D^2 = \{x \in \mathbb{R}^2 | \|x\| \leq \delta\}$ with radius δ, starting at a point s and having direction s'. We construct an environment E by sweeping the disk along a constant κ' curvature curve ϕ, connecting (s, s') to (s, s'), whereby $\kappa' > \kappa$. Let us now look at the motion planning problem of planning for D^2 from (s, s') to a point (p, p'), with $(p, p') \in E$. Visualized in Fig. 9. Since the environment is not intersecting the boundary of the cone P_0, which is constructed by s, s', κ', it follows from Theorem 4 that no function can reach (p, p'). ■

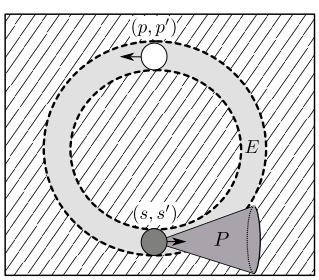

Fig. 9: Visualization of a simple completeness counterexample, in which an environment E has to be solved, which follows a $\kappa' > \kappa$ curvature curve.

We established so far that if we can find a feasible trajectory for link L_0 under a curvature constraint, then we can find a trajectory for the whole linear linkage, which is feasible. We showed that this is not complete, however we can define a weaker version of completeness, which we call κ-curvature completeness

Definition 8. *A motion planning algorithm is κ-curvature complete if it finds a trajectory in the functional space $\mathcal{F}_{\kappa_0} \subset \mathcal{F}$, if one exists, or correctly reports that no such exist.*

We observe that this is a weaker version, such that completeness would imply κ-curvature completeness, but not the other way round. This is depicted schematically in Fig. 10.

The next section will be devoted to develop a κ-curvature complete algorithm.

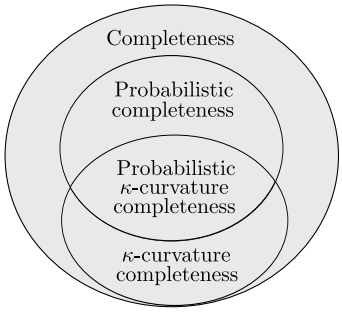

Fig. 10: The κ-curvature completeness property and its relation to probabilistic completeness and completeness.

V. Irreducible Curvature Complete Algorithm

In Theorem 5, we established that a linear linkage $\mathcal{R}_L^N$ with links $L_0 \to \cdots \to L_N$ has a feasible solution if we can find a feasible solution for L_0 which respects a certain curvature κ. Here, we describe an algorithm to compute this solution. We will use spherical joints for the sublinks, such that we have joint configurations $\theta_1, \cdots, \theta_N, \gamma_1, \cdots, \gamma_N$.

Now, given a trajectory $\tau \in \mathcal{F}_{\kappa_N}$ for L_0, we compute feasible joint configurations for the sublinks $L_1, \cdots, L_N$. A rotational joint can be seen as a special case with $\gamma_1 \cdots, \gamma_N = 0$.

Let $A = \{\mathcal{R}_L^N, \mathcal{C}, q_I, q_G, \mathbf{E}\}$ be a motion planning problem for $\mathcal{R}_L^N$. Let $\tau \in \mathcal{F}_{\kappa_N}$ be the trajectory of the root link L_0. If $\tau \oplus L_0$ is a feasible solution, then by Theorem 5 we are guaranteed to find a feasible configuration such that $\tau \oplus (L_0 \cup \cdots \cup L_N)$ is a feasible solution. We will describe now how to find the configurations given a trajectory $\tau \in \mathcal{F}_{\kappa_N}$.

For all $t_0 \in [0, 1]$ we compute θ_1 by the following procedure: start at $\tau(t_0)$ and move along τ in backward direction. See Fig. 12. Since we are guaranteed by Theorem 3 that we will meet ∂P_0, we can denote the intersection point as $t_n < t_0$ with $\|\tau(t_n) - \tau(t_0)\| = l_0$. Then we have

$$\theta = \operatorname{acos}\left(\frac{-\tau'(t_0)^T(\tau(t_n) - \tau(t_0))}{\|\tau'(t_0)\|\|\tau(t_n) - \tau(t_0)\|}\right) \tag{18}$$

from t_q we recursively compute all θ values.

As a technical detail, we note that this requires that even at q_I, we can follow the trajectory backwards. Therefore, we

need to extend the trajectory by moving along the sublinks at q_I to obtain an extended trajectory $\tau = \tau_I \circ \tau$.

The resulting algorithm is described in Fig. 11. It takes the input trajectory τ and produces a resulting configuration vector at each instance $t \in [0,1]$ along τ, such that the resulting swept volume of all links is inside the swept volume of the root link, i.e. $(\tau \oplus L_0 \cup \cdots \cup L_N) \subseteq (\tau \oplus L_0)$. The complexity scales with $\mathcal{O}(N)$. The algorithm has been implemented in python and is available as a standalone module

https://github.com/orthez/irreducible-curvature-projection/

Algorithm 1: Irreducible Curvature Projection

Data: $t_0, \tau, \tau', \tau'', \delta_{0:N}, l_{1:N}, \Delta t$
Result: $\theta_{1:N}, \gamma_{1:N}$
$\mathbf{e}_1 \leftarrow \tau'(t_0)$;
$\mathbf{e}_2 \leftarrow \tau''(t_0)$;
$\mathbf{e}_3 \leftarrow \tau'(t_0) \times \tau''(t_0)$;
$t_{cur} \leftarrow t_0$;
$\mathbf{R} \leftarrow \begin{pmatrix} \mathbf{e}_1 \cdot \mathbf{e}_x & \mathbf{e}_2 \cdot \mathbf{e}_x & \mathbf{e}_3 \cdot \mathbf{e}_x \\ \mathbf{e}_1 \cdot \mathbf{e}_y & \mathbf{e}_2 \cdot \mathbf{e}_y & \mathbf{e}_3 \cdot \mathbf{e}_y \\ \mathbf{e}_1 \cdot \mathbf{e}_z & \mathbf{e}_2 \cdot \mathbf{e}_z & \mathbf{e}_3 \cdot \mathbf{e}_z \end{pmatrix}$;
for $i \leftarrow 1$ **to** N **do**
  $t_n \leftarrow t_0$;
  while $\|\tau(t_n) - \tau(t_{cur})\| \leq l_i$ **do**
    $t_n \leftarrow t_n - \Delta t$
  $\tau_n \leftarrow \tau(t_n)$;
  $p_I \leftarrow \tau(t_n) - \tau(t_{cur})$;
  $p_W \leftarrow \mathbf{R}^T p_I$;
  $x_L \leftarrow (-1, 0, 0)^T$;
  $p_{xy} \leftarrow p_W - (p_W^T \mathbf{e}_z)\mathbf{e}_z$;
  $p_{zx} \leftarrow p_W - (p_W^T \mathbf{e}_y)\mathbf{e}_y$;
  $\theta_i \leftarrow \operatorname{acos}(\frac{p_{xy} x_L}{\|p_{xy}\| \|x_L\|})$;
  $\gamma_i \leftarrow \operatorname{acos}(\frac{p_{zx} x_L}{\|p_{zx}\| \|x_L\|})$;
  if $p_W^T \mathbf{e}_z < 0$ **then**
    $\gamma_i \leftarrow -\gamma_i$;
  if $p_W^T \mathbf{e}_y > 0$ **then**
    $\theta_i \leftarrow -\theta_i$;
  $\mathbf{R} \leftarrow \mathbf{R} \cdot \mathbf{R}_Y(\gamma_i) \cdot \mathbf{R}_Z(\theta_i)$;
  $\mathbf{e}_1 \leftarrow \mathbf{R}\mathbf{e}_x$;
  $\mathbf{e}_2 \leftarrow \mathbf{R}\mathbf{e}_y$;
  $\mathbf{e}_3 \leftarrow \mathbf{R}\mathbf{e}_z$;
  $t_{cur} \leftarrow t_n$;

Fig. 11: Irreducible Curvature Projection Algorithm. $\mathbf{e}_x, \mathbf{e}_y, \mathbf{e}_z$ represent the x, y, z basis vectors, respectively.

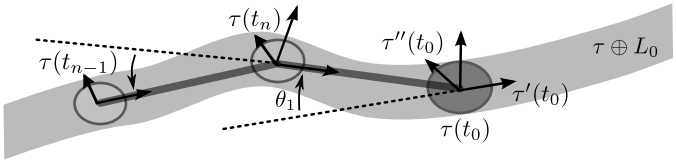

Fig. 12: Given a trajectory $\tau \in \mathcal{F}_{\kappa_N}$, we can analytically compute the joint configurations, such that sublinks of the linear linkage are reduced, i.e. they are inside of the swept volume of $\tau \oplus L_0$..

A. Irreducibility Assurance Controller

The analytical computation of the irreducible configuration at instance t enables us to design a control algorithm, which pushes the robot body towards an irreducible trajectory.

Let us denote by $\phi : \mathcal{F} \times [0,1] \to \mathbb{R}^N \times \mathbb{R}^N$ the computation of joint angles for our spherical joint from the current trajectory $\tau \in \mathcal{F}$ of body L_0 at instance $t_0 \in [0,1]$. The output are joint angles θ, γ specifying the position of the spherical joints at instance t_0. Let us denote by $\varphi : [0,1] \to \mathbb{R}^N \times \mathbb{R}^N$ the *measured joint angles* at instance $t_0 \in [0,1]$.

A proportional gain controller can be constructed as $u(t) = K_p e(t)$ with $e(t) = \|\phi(t) - \varphi(t)\|$. This gives a hint at the possibilities of this geometrical inspired approach. In general, using the controller will minimize the swept volume, which could be useful in different areas. We note that minimal swept volume loosely relates to minimal air resistance. For example, an octopus robot could use this to let the arms trail behind its body while moving, such that water resistance is minimized. A road train — a tractor unit pulling two or more trailers — could minimize its air resistance to minimize gas consumption.

VI. Experiments

We performed two experiments to verify our theoretical results. First, a swimming snake in a 2d and a 3d environment. Planning is conducted for the head of the snake under a curvature constraint. After finding a feasible head trajectory we can use the Irreducible Curvature Projection Algorithm to project the remaining sublinks into the swept volume of the head. Second, we planned a constrained motion for the humanoid robot HRP-2, where we plan a motion for a reduced mechanical model with 7 dimensions. After planning a motion, we then use our projection algorithm to find the position of the remaining links.

A. Swimming Snake

For the snake simulation, we have choosen a bounded curvature, and estimated the number of links, such that we obtain the longest possible irreducible snake. Our values were $\kappa = 1\text{m}^{-1}$, $\delta_0 = 0.23\text{m}$, $\delta_i = 0.138\text{m}$, $l_0 = 0.33\text{m}$ and $\theta^L = \frac{\pi}{2}$ giving rise to

$$N = \left\lfloor \frac{2\sin(\theta^L)}{\kappa l_0} \right\rfloor = 6 \tag{19}$$

Planning with our curvature-constrained functional space is equivalent to planning a path for the non-holonomic snake's head subject to differential constraints describing forward non-slipping motions and for which we will assume constant speed. Note that this is equivalent to the model of Dubin's car. This can be solved in both 2d and 3d using kinodynamic planning [25].

In 2d, the configuration space of the snake's head is $SE(2)$ with $q = (x, y, \theta)^T$ and the differential model is given by

$$\begin{aligned} \dot{x} &= \cos\theta \\ \dot{y} &= \sin\theta \\ \dot{\theta} &= u \end{aligned} \tag{20}$$

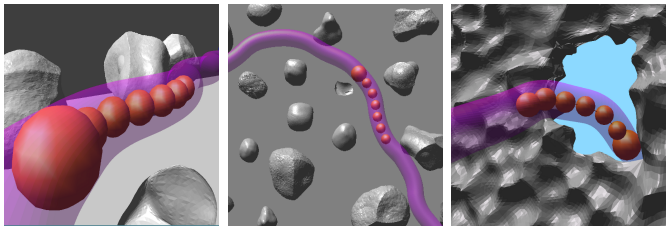

Fig. 13: Planning for the head of a swimming snake in 2D (left, middle), and in 3d (right). The swept volume of the head is shown in magenta. The position of the sublinks is an output of the curvature projection algorithm.

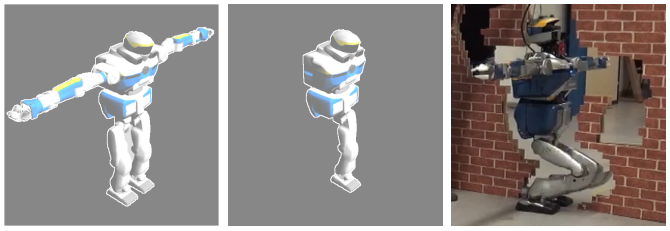

Fig. 14: We use a reduced mechanical model for motion planning, which preserves curvature completeness for the linear arm linkages with respect to the chest (left,middle). After planning for the reduced model, we can project the remaining links into the swept volume, and thereby solving very narrow environments (right, adapted from [27]).

where the control space is defined by the steering angle u. In 3d, the configuration space is $SE(3)$ and the differential model is similar to a driftless airplane given by

$$\dot{q} = q\left(\sum_{i=1}^{3} u_i X_i + X_4\right) \tag{21}$$

where

$$X_1 = \begin{bmatrix} 0 & 0 & 0 & 0 \\ 0 & 0 & -1 & 0 \\ 0 & 1 & 0 & 0 \\ 0 & 0 & 0 & 0 \end{bmatrix} \quad X_2 = \begin{bmatrix} 0 & 0 & 1 & 0 \\ 0 & 0 & 0 & 0 \\ -1 & 0 & 0 & 0 \\ 0 & 0 & 0 & 0 \end{bmatrix} \quad X_3 = \begin{bmatrix} 0 & -1 & 0 & 0 \\ 1 & 0 & 0 & 0 \\ 0 & 0 & 0 & 0 \\ 0 & 0 & 0 & 0 \end{bmatrix}$$

$$X_4 = \begin{bmatrix} 0 & 0 & 0 & 1 \\ 0 & 0 & 0 & 0 \\ 0 & 0 & 0 & 0 \\ 0 & 0 & 0 & 0 \end{bmatrix} \quad X_5 = \begin{bmatrix} 0 & 0 & 0 & 0 \\ 0 & 0 & 0 & 1 \\ 0 & 0 & 0 & 0 \\ 0 & 0 & 0 & 0 \end{bmatrix} \quad X_6 = \begin{bmatrix} 0 & 0 & 0 & 0 \\ 0 & 0 & 0 & 0 \\ 0 & 0 & 0 & 1 \\ 0 & 0 & 0 & 0 \end{bmatrix}$$

is a basis for $\mathfrak{se}(3)$, the Lie algebra of $SE(3)$.

The controls u_1, u_2 and u_3 are then the roll, pitch and yaw steering angles, respectively. We have performed one experiment in 2d in a rocky environment, and averaged the results for the classical and the irreducible case over 100 experiments, as reported in Tab. III. While having the same success rate, the planning time is reduced by one order of magnitude. We further planned a single motion in 3d, where the snake has to swim through holes in a formation of rocks. Fig. 13 shows the results of our projection algorithm with the swept volume of the head in magenta.

B. Humanoid Robot

Next, we conduct motion planning for the humanoid robot HRP-2, by abstracting away the two arms as linear linkages. Also, we consider the right leg as a linear linkage connected to the left leg. We additionally approximate the head by a sphere, so that yaw rotations leave the head invariant. This leaves us with an effective configuration space of $\mathbb{R}^7$, which is shown in Table I. Motion planning can now be conducted with a *reduced* mechanical model, as shown in Fig. 14.

TABLE I: Variable Joints of Humanoid Robot HRP-2, and the corresponding range. If the value is set to ϕ, then the joints are ignored for motion planning, and are determined by the irreducible projection algorithm in a post-processing stage.

Joint	Fixed Value	Anatomical Name	Range
HEAD0	0.0		
HEAD1	-	Neck	$[-0.52, 0.79]$
CHEST0	0.0		
CHEST1	-	Waist	$[-0.09, 1.05]$
RARM	ϕ	Right Arm	
LARM	ϕ	Left Arm	
LLEG0	0.0		
LLEG1	0.0		
LLEG2	-	Hip	$[-2.18, 0.73]$
LLEG3	-	Knee	$[-0.03, 2.62]$
LLEG4	-	Ankle	$[-1.31, 0.73]$
LLEG5	0.0		
RLEG	ϕ	Right Leg	
LSOLE_X	-	Left Foot	$[-0.5, 0.5]$
LSOLE_Y	-	Left Foot	$[-3.0, 3.0]$
LSOLE_θ	-	Left Foot	$[0, 2\pi]$

TABLE II: Values for the approximated linear linkage structure of the arms of HRP-2. Our curvature algorithm determines the exact values based on the movement of the chest.

Joint	0	1	2	3	4	5	6
Left Arm	$\frac{-\pi}{2}$	$[\frac{\pi}{4}, \frac{3\pi}{4}]$	$\frac{-\pi}{2}$	$[\frac{-\pi}{4}, \frac{\pi}{4}]$	0.0	$[\frac{-\pi}{4}, \frac{\pi}{4}]$	0.1
Right Arm	$\frac{-\pi}{2}$	$[\frac{-3\pi}{4}, \frac{-\pi}{4}]$	$\frac{-\pi}{2}$	$[\frac{-\pi}{4}, \frac{\pi}{4}]$	0.0	$[\frac{-\pi}{4}, \frac{\pi}{4}]$	0.1

1) Curvature constraint for chest HRP-2: Each arm of HRP-2 is a linear linkage, which we will approximate by four spheres as depicted in Fig. 15. We positioned the spheres at the moveable joints of the robot. The resulting linear linkage has $N = 4$ links with length $L_0 = 0.25\text{m}$ and sphere radius of $\delta = 0.08\text{m}$. We choose a common joint interval $[-\frac{\pi}{4}, \frac{\pi}{4}]$ for the free joints. We can compute the resulting maximum curvature as

$$\kappa = \frac{2\sin(\frac{\pi}{4})}{3L_0} = 1.8856\text{m}^{-1} \tag{22}$$

Meaning, if we can find a trajectory of the chest (without considering the arms), which has a bounded κ curvature, then we are guaranteed to find joint angles for the arm, such that the swept volume of the arms and the chest is a subset of the swept volume of the chest. The resulting joint limits for the arms of HRP-2 are shown in Table II.

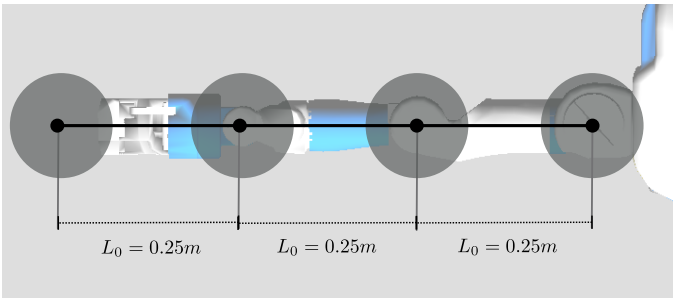

Fig. 15: Approximation of the arm as a linear linkage in canonical form

2) Implementation Details: For our simulations, we use the humanoid path planner (HPP) framework [28]. It is a general motion planning framework based on random sampling techniques [25], tailored for planning on humanoid robots like HRP-2. We will make use of a planning algorithm based on sliding motions. A sliding motion is dynamically stable, as we discussed in Sec. II, and is particulary suitable for constrained environment as it locally minimizes the swept volume by minimizing oscillations. From a motion planning point of view, a sliding motion is easier to deal with computationally: while planning discrete contact steps gives rise to a combinatorial explosion, a continuous sliding motion can be optimized by taking derivative informations into account.

To plan a single motion, we use the rapidly-exploring tree (RRT) [29] algorithm. We replace the basic configuration shooter, which samples a random configuration from the configuration space by an irreducible configuration shooter, to only sample inside the subspace generated by ignoring the arms and the right leg. After planning, we compute the reduced configurations by using the irreducible curvature projection algorithm.

The irreducible configuration shooter has been released as an open-source submodule for the HPP framework, which can be found here

https://github.com/orthez/hpp-motion-prior/

3) Experimental Results: To test our theoretical results, we have chosen a motion planning problem, where the robot HRP-2 has to move through a wall, as shown in Fig. 16. Those results have been taken from [1]. Due to the wall constraint, a solver has to find a narrow passage in the configuration space to solve the problem. In the classical 35-dof setting, this problems has not been solved, since in practice the probability to find a feasible configuration vanishes towards zero. We consider here the 7-dof setting without waypoints, by using the irreducible subspace.

The results of 10 runs are reported in Table III. Since the passage is narrow, RRT can take a long time to converge, for our experiment, it took between 44 minutes up to 43 hours. This shows that sampling-based methods are becoming inefficient in narrow environments, which is closely related to the ϵ-goodness criteria [30], which states that the convergence rate of sampling-based methods is inversly proportional to the volume of the free configuration space.

We have successfully applied the irreducibility concept on the HRP-2 humanoid walk through the wall. This experiment, however, uses a different planning algorithm which exploits environmental structure, and follows the resulting trajectory by using a hierarchical task-space controller. We submitted those results in [27].

Since this paper is concerned with a feasibility study, the resulting motion will be non-optimal, assumes infinitesimal small footsteps and might appear unnatural to a human observer. However, having a first feasible trajectory is a prerequisite for fast convergence of local planning algorithms like CHOMP [31] or AICO [32].

TABLE III: Simulation results for the snake and for the humanoid robot. The "snake 2d Rocks" and "Snake 3d Rock Formation" refers to the environment shown in Fig. 13. *HRP-2 Wall* refers to the experiment in Fig. 16. Results taken from [1].

Planning Problem	$\mathcal{C}$ Dimension	#Success/ #Experiments	σ(s)	μ(s)
Snake 2d Rocks (Classical)	$\mathbb{R}^{3+N}$	100/100	54.15s	94.36s
Snake 2d Rocks (Irreducible)	$\mathbb{R}^3$	100/100	1.34s	1.04s
HRP-2 Wall (Classical)	$\mathbb{R}^{35}$	Not solveable ($>$ 3days)		
HRP-2 Wall (Irreducible) [1]	$\mathbb{R}^7$	10/10	12h14m	9h34m

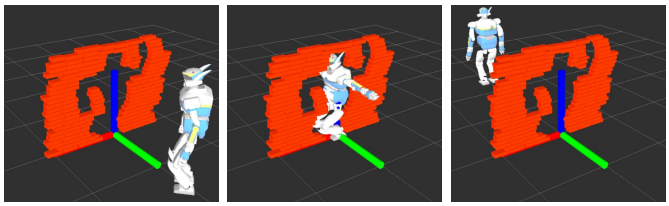

Fig. 16: Wall Motion Planning Problem. **Left** initial configuration **Middle** one irreducible configuration on the final trajectory found by an RRT on the irreducible subspace **Right** goal configuration. Adapted from [1].

VII. Discussion

The theoretical framework presented is able to simplify motion planning problems by exploiting the linear linkage structure, which can be found in a diverse number of mechanical systems, including snakes, octopuses and humanoid robots.

Our conceptual idea is a completeness-preserving dimensionality reduction technique. To apply this concept in practice, we introduced a new concept called κ-curvature completeness. This κ-curvature completeness is in general a proper subset of completeness, and therefore we can always find certain situations in which we cannot find a solution, even if one exists. We believe, however, that for some mechanical systems κ-curvature completeness and completeness are equivalent, for example for systems which resemble Dubin's car with trailers and positive velocity.

Motion planning can now be simplified by first planning under a certain curvature constraint in the reduced dimensionality space. If a motion plan has been found, we can execute it. If no plan has be found, we can increase the dimensionality.

In the larger scheme, we think about irreducibility as one component of *motion prior* information: developing efficient motion planning algorithms requires us to make use of the underlying structure of the problem. Here, we showed that certain mechanical systems allow us to exploit their linear linkage structure.

Finally, it seems that linear linkages are quite common in nature. Irreducibility could be a way to motivate why the octopus aligns its limbs behind its head during swimming. Besides minimizing water resistance, it could also thereby simplify motion planning. We think there is a variety of interesting phenomena which could be studied by exploiting

our concept of an irreducible trajectory in motion research.

VIII. Conclusion

We described the concept of irreducibility, which allows us to conduct completeness-preserving dimensionality reduction for motion planning. The main result in Theorem 2 states that finding no feasible trajectory in the space of irreducible trajectories implies that there is no feasible trajectory in the space of all configuration space trajectories, i.e. that motion planning is complete w.r.t. irreducible trajectories.

We have described how irreducibility can be applied to linear linkages by using the concept of κ-curvature completeness. Based on those results, we developed a linear-time algorithm to project configurations into the swept volume of the root links of a linear linkage. Finally, we conducted a set of experiments for the humanoid robot HRP-2, by considering the arms as linear linkages.

Future research will focus on the automatic discovery of the irreducible trajectory space, on the correctness of the conjectures in Sec. IV-F, and on applying our principle to more general linkage structures.

Appendix

Proofs

Proof of Theorem 1: Let $s = \mathcal{SV}(\tau)$ and $s' = \mathcal{SV}(\tau')$. s is feasible if $s \cap \mathbf{E} = \emptyset$. We proceed by direct proof:
(1) Let s be infeasible, then $\exists v \in s$, such that $v \cap \mathbf{E} = v$. Since $s \subset s'$, we have that $v \in s'$. Since v exists, we can conclude that at least $s' \cap \mathcal{E} > v$, which makes s' infeasible.
(2) τ' being feasible means $s' \cap \mathbf{E} = \emptyset$. Since $s \subset s'$, it follows from elementary set theory that $s \cap \mathbf{E} = \emptyset$, which proofs that τ is feasible. ∎

Proof of Lemma 1: Let μ be the lebesque measure on the workspace $\mathcal{W}$. First, let us see that if $\mathcal{SV}(\tau_1) \subset \mathcal{SV}(\tau_0)$, then $\mu(\mathcal{SV}(\tau_1)) < \mu(\mathcal{SV}(\tau_0))$.

Now, by definition, if $\tau_0 \notin \mathcal{I}$, then $\exists \tau_1 \in \mathcal{F}$, such that $\mathcal{SV}(\tau_1) \subset \mathcal{SV}(\tau_0)$. Then either $\tau_1 \in \mathcal{I}$, and we are done. Or $\tau_1 \notin \mathcal{I}$, and by definition, $\exists \tau_2 \in \mathcal{F}$, such that $\mathcal{SV}(\tau_2) \subset \mathcal{SV}(\tau_1)$. Let us assume that there is no trajectory $\tau_i \in \mathcal{I}$, such that we obtain an infinite sequence $\Pi = \{\tau_0, \tau_1, \tau_2, \cdots\}$ of reducible trajectories $\tau_i \in \mathcal{F}$, such that $\forall \tau_i \in \Pi : \mathcal{SV}(\tau_{i+1}) \subset \mathcal{SV}(\tau_i)$. Since we have $\forall \tau_i \in \Pi : \mu(\mathcal{SV}(\tau_{i+1})) < \mu(\mathcal{SV}(\tau_i))$ and $\mu(\mathcal{SV}(\tau)) > 0$, the sequence is strictly monotonically decreasing and bounded, and will therefore converge to its maximum lower bound, which we call C, i.e. $\lim_{n\to\infty} \mu(\mathcal{SV}(\tau_i)) = C$. Consequently, since the maximum lower bound is obtained, there cannot exists another trajectory τ', such that $\mu(\mathcal{SV}(\tau')) < C$. By definition, the sequence is converged in $\mathcal{I}$, and therefore we conclude that every element $\tau \in \mathcal{F} \setminus \mathcal{I}$ is reducible by $\tau' \in \mathcal{I}$. ∎

Proof of Theorem 2:

Let us assume that $\exists \tau \in \mathcal{F}$, with τ being feasible, and that $\forall \tau' \in \mathcal{I} : \tau'$ is not feasible. Since τ is feasible, it follows that $\tau \notin \mathcal{I}$. Then by definition there has to be a $\tau'' \in \mathcal{F}$ such that $\mathcal{SV}(\tau'') \subset \mathcal{SV}(\tau)$. Then τ'' is feasible by Theorem 1. Further, either we have that $\tau'' \in \mathcal{I}$. Then we have a contradiction. Or we have $\tau'' \notin \mathcal{I}$, which means that we can still find another $\tau''' \in \mathcal{F}$ reducing τ''. By Lemma 1, we know that such a sequence can be reduced by a $\tilde{\tau} \in \mathcal{I}$. So we reach a contradiction, too. ∎

Proof of Corollary 1: By definition, motion planning is complete, if we can find a solution (a trajectory), if one exist. By Theorem 2, we know that if we cannot find a solution in $\mathcal{I}$, then there is no solution in $\mathcal{F}$. Conversely, if there is a solution in $\mathcal{F}$, then by Theorem 1, there exists a solution in $\mathcal{I}$. ∎

References

[1] A. Orthey, F. Lamiraux, and O. Stasse, "Motion Planning and Irreducible Trajectories," in *International Conference on Robotics and Automation*, 2015.

[2] M. Spivak, *A comprehensive introduction to differential geometry. Vol. I*. Publish or Perish Inc., 1979.

[3] K. Y. Kensuke Harada, Eiichi Yoshida, ed., *Motion Planning for Humanoid Robots*. Springer, 2010.

[4] N. Vahrenkamp, D. Berenson, T. Asfour, J. Kuffner, and R. Dillmann, "Humanoid motion planning for dual-arm manipulation and re-grasping tasks," in *International Conference on Intelligent Robots and Systems*, 2009.

[5] A. Escande, A. Kheddar, and S. Miossec, "Planning contact points for humanoid robots," *Robotics and Autonomous Systems*, vol. 61, no. 5, pp. 428 – 442, 2013.

[6] Y. Zhang, J. Luo, K. Hauser, H. A. Park, M. Paldhe, C. Lee, R. Ellenberg, B. Killen, P. Oh, J. H. Oh, *et al.*, "Motion planning and control of ladder climbing on DRC-Hubo for DARPA Robotics Challenge," in *International Conference on Robotics and Automation*, 2014.

[7] A. El Khoury, F. Lamiraux, and M. Taix, "Optimal Motion Planning for Humanoid Robots," in *International Conference on Robotics and Automation*, 2013.

[8] K. Hauser, T. Bretl, K. Harada, and J.-C. Latombe, "Using motion primitives in probabilistic sample-based planning for humanoid robots," in *Algorithmic foundation of robotics VII*, pp. 507–522, Springer, 2008.

[9] R. Deits and R. Tedrake, "Footstep Planning on Uneven Terrain with Mixed-Integer Convex Optimization," in *International Conference on Humanoid Robots*, 2014.

[10] S. Hirose and H. Yamada, "Snake-like robots [Tutorial]," *Robotics and Automation Magazine*, 2009.

[11] E. S. Conkur and R. Gurbuz, "Path Planning Algorithm for SnakeLike Robots," *Information Technology And Control*, vol. 37, no. 2, pp. 159–162, 2008.

[12] J. Liu, Y. Wang, B. Ii, and S. Ma, "Path planning of a snake-like robot based on serpenoid curve and genetic algorithms," in *Intelligent Control and Automation*, 2004.

[13] W. Henning, F. Hickman, and H. Choset, "Motion Planning for Serpentine Robots," in *Proceedings of ASCE Space and Robotics*, 1998.

[14] D. Rollinson and H. Choset, "Virtual Chassis for Snake Robots," in *International Conference on Intelligent Robots and Systems*, 2011.

[15] E. Cappo and H. Choset, "Planning end effector trajectories for a serially linked, floating-base robot with changing support polygon," in *American Control Conference*, 2014.

[16] S. Dalibard and J.-P. Laumond, "Linear Dimensionality Reduction in Random Motion Planning," *International Journal of Robotics Research*, 2011.

[17] M. Ciocarlie, C. Goldfeder, and P. Allen, "Dimensionality reduction for hand-independent dexterous robotic grasping," in *International Conference on Intelligent Robots and Systems*, 2007.

[18] P. Allen, M. Ciocarlie, and C. Goldfeder, "Grasp planning using low dimensional subspaces," in *The Human Hand as an Inspiration for Robot Hand Development* (R. Balasubramanian and V. J. Santos, eds.), Springer Tracts in Advanced Robotics, Springer International Publishing, 2014.

[19] A. Mahoney, J. Bross, and D. Johnson, "Deformable robot motion planning in a reduced-dimension configuration space," in *International Conference on Robotics and Automation*, 2010.

[20] I. Kabul, R. Gayle, and M. C. Lin, "Cable route planning in complex environments using constrained sampling," in *ACM Symposium on Solid and Physical Modeling*, ACM, 2007.

[21] S. Bereg and D. Kirkpatrick, "Curvature-bounded traversals of narrow corridors," in *Symposium on Computational geometry*, ACM, 2005.
[22] H.-K. Ahn, O. Cheong, J. Matouek, and A. Vigneron, "Reachability by paths of bounded curvature in a convex polygon," *Computational Geometry*, 2012.
[23] S. Guha and S. D. Tran, "Reconstructing curves without delaunay computation," *Algorithmica*, 2005.
[24] S. Dalibard, A. Khoury, F. Lamiraux, M. Taix, and J. Laumond, "Small-Space Controllability of a Walking Humanoid Robot," in *International Conference on Humanoid Robots*, 2011.
[25] S. M. LaValle, *Planning Algorithms*. Cambridge University Press, 2006.
[26] P. K. Agarwal, T. Biedl, S. Lazard, S. Robbins, S. Suri, and S. Whitesides, "Curvature-constrained shortest paths in a convex polygon," *SIAM Journal on Computing*, 2002.
[27] A. Orthey, V. Ivan, M. Naveau, Y. Yang, O. Stasse, and S. Vijayakumar, "Homotopic Particle Motion Planning for Humanoid Robotics." Submitted to International Conference on Intelligent Robots and Systems (IROS), 2015.
[28] F. Lamiraux and J. Mirabel, "HPP: a new software framework for manipulation planning." Submitted to International Conference on Intelligent Robots and Systems, 2015.
[29] S. M. Lavalle and J. J. Kuffner Jr, "Rapidly-Exploring Random Trees: Progress and Prospects," in *Algorithmic and Computational Robotics: New Directions*, 2000.
[30] L. E. Kavraki, J.-C. Latombe, R. Motwani, and P. Raghavan, "Randomized query processing in robot path planning," in *Symposium on Theory of Computing*, pp. 353–362, ACM, 1995.
[31] M. Zucker, N. Ratliff, A. Dragan, M. Pivtoraiko, M. Klingensmith, C. Dellin, J. A. D. Bagnell, and S. Srinivasa, "CHOMP: Covariant Hamiltonian Optimization for Motion Planning," *International Journal of Robotics Research*, May 2013.
[32] M. Toussaint, "Robot trajectory optimization using approximate inference," in *International Conference on Machine Learning*, 2009.